**Title**
Mouse Cntnap2 and Human CNTNAP2 ASD Alleles Cell Autonomously Regulate PV+ Cortical Interneurons.

**Authors**
Vogt, Daniel
Cho, Kathleen KA
Shelton, Samantha M
et al.

ORIGINAL ARTICLE

# Mouse *Cntnap2* and Human *CNTNAP2* ASD Alleles Cell Autonomously Regulate PV[+] Cortical Interneurons

Daniel Vogt[1], Kathleen K. A. Cho[1], Samantha M. Shelton[1], Anirban Paul[2], Z. Josh Huang[2], Vikaas S. Sohal[1] and John L. R. Rubenstein[1]

[1]Department of Psychiatry, University of California San Francisco, San Francisco, CA 94158, USA and [2]Cold Spring Harbor Laboratory, Cold Spring Harbor, NY 11724, USA

Address correspondence to Daniel Vogt and John L. R. Rubenstein. Email: Vogtdan2@msu.edu (D.V.); John.rubenstein@ucsf.edu (J.R.).

Daniel Vogt, Kathleen K. A. Cho and Samantha M. Shelton contributed equally to this work

## Abstract

Human mutations in *CNTNAP2* are associated with an array of neuropsychiatric and neurological syndromes, including speech and language disorders, epilepsy, and autism spectrum disorder (ASD). We examined *Cntnap2*'s expression and function in GABAergic cortical interneurons (CINs), where its RNA is present at highest levels in chandelier neurons, PV^{+} neurons and VIP^{+} neurons. In vivo functions were studied using both constitutive *Cntnap2* null mice and a transplantation assay, the latter to assess cell autonomous phenotypes of medial ganglionic eminence (MGE)-derived CINs. We found that *Cntnap2* constitutive null mutants had normal numbers of MGE-derived CINs, but had reduced PV[+] CINs. Transplantation assays showed that *Cntnap2* cell autonomously regulated the physiology of parvalbumin (PV)[+], fast-spiking CINs; no phenotypes were observed in somatostatin[+], regular spiking, CINs. We also tested the effects of 4 human *CNTNAP2* ASD missense mutations in vivo, and found that they impaired PV[+] CIN development. Together, these data reveal that reduced *CNTNAP2* function impairs PV[+] CINs, a cell type with important roles in regulating cortical circuits.

**Key words:** CNTNAP2, Cortical interneuron, fast-spiking, MGE, parvalbumin

## Introduction

Human *CNTNAP2* encodes the CASPR2 protein, a member of the neurexin family of cell adhesion molecules. In recent years, the scope of human disorders associated with *CNTNAP2* has grown (for reviews see: Rodenas-Cuadrado et al. 2014; Poot 2015, 2017). Notably, *CNTNAP2* dysfunction in humans has been implicated in speech and language disorders, including Gilles de la Tourette syndrome, stuttering, and selective mutism (Verkerk et al. 2003; Petrin et al. 2010; Stein et al. 2011; Zhao et al. 2015). Notably, there is evidence that *CNTNAP2* is directly repressed by *FoxP2*, a gene implicated in speech and language disorders. In addition, *CNTNAP2* mutations have been discovered in individuals with cortical dysplasia-focal epilepsy syndrome (Strauss et al. 2006), Pitt-Hopkins like syndrome (Zweier et al. 2009), Schizophrenia (Friedman et al. 2008; Ji et al. 2013), obsessive compulsive disorder (Verkerk et al. 2003), attention deficit hyperactivity disorder (Elia et al. 2010) as well as autism spectrum disorder (ASD) (Alarcon et al. 2008; Arking et al. 2008; Bakkaloglu et al. 2008; Poot et al. 2010).

In mice and zebrafish, *Cntnap2* has been implicated in many biological processes, including clustering potassium channels at the juxtaparanodes of myelinated axons, trafficking Glutamatergic AMPA receptors, positively regulating synaptic strength and the number of GABAergic neurons (Horresh et al. 2008; Anderson et al. 2012; Varea et al. 2015; Hoffman et al. 2016).

*Cntnap2* is broadly expressed in the developing and mature central nervous system (Gordon et al. 2016). Due to the number of disorders implicated in *CNTNAP2* dysfunction, one idea is that CASPR2 may serve as a hub at the cell membrane that

integrates multiple brain regions and coordinates several developmental and maturational processes through its association with both extracellular- and intracellular-binding partners (Rodenas-Cuadrado et al. 2014; Poot 2015, 2017).

Of note, recent reports have implicated *CNTNAP2* in inhibitory (GABAergic) neuron development/maturation. While cortical excitation is primarily mediated by glutamatergic projection neurons and thalamic afferents, cortical inhibition is primarily mediated by locally projecting GABAergic cortical interneurons (CINs) and basal telencephalic GABAergic projection neurons. CINs have diverse morphologies, molecular makeup and electrophysiological properties; they mediate inhibition in distinct ways (Wonders and Anderson 2006; Kepecs and Fishell 2014; Kessaris et al. 2014). For instance, parvalbumin (PV)$^+$ basket CINs are fast spiking, and innervate the cell body of pyramidal neurons, whereas chandelier neurons (many of which are PV$^+$) innervate the initial axon segment (Huang et al. 2007). Mouse mutants lacking *Cntnap2* have been reported to have decreased CINs, including the parvalbumin (PV)+, neuropeptide-Y (NPY)+, and calretinin (CR)+ subgroups (Peñagarikano et al. 2011). Moreover, the number of GABAergic neurons is decreased in zebrafish with *Cntnap2* deletion (Hoffman et al. 2016). Interestingly, loss of function of another neurexin family member, *Cntnap4*, led to decreased GABAergic activity and increased dopaminergic activity, and resulted in PV$^+$ CINs that had dampened firing properties (Karayannis et al. 2014). These data suggest that *CNTNAP* family members may control aspects of CIN development/maturation. However, little is known about *CNTNAP2*'s function within CINs, in part because of its broad expression, making it impossible to ascertain its cell autonomous functions in the *Cntnap2* constitutive null mouse.

Deficits in CINs have been identified in both humans diagnosed with ASD patients and in genetic animal models of ASD (Peñagarikano et al. 2011; Han et al. 2012; Karayannis et al. 2014; Vogt, Cho et al. 2015; Hoffman et al. 2016; Hashemi et al. 2017). Thus, it is important to rigorously establish whether and how human neurological disease risk genes regulate CIN development and function. Moreover, many types of mutations (e.g., nonsense, missense, and synonymous) have been discovered in humans with neuropsychiatric disorders but their potentially diverse impacts on protein function is not well understood. Of note, missense mutations have been the most difficult to evaluate as they are not obviously deleterious. Notably, in some individuals both alleles of *CNTNAP2* are mutated and are either known to, or predicted to, lead to no functional protein (Strauss et al. 2006; Zweier 2012; Watson et al. 2014; Rodenas-Cuadrado et al. 2016). While these and other mutations discovered in *CNTNAP2* have been either studied in detail or predicted to be deleterious, there are many missense mutations for which little is known. In addition, there is little understanding as to whether these mutations result in functional changes in *CNTNAP2*. Moreover, the role that *CNTNAP2* dysfunction may play in ASD symptoms is still under investigation.

Herein, *CNTNAP2* function was assessed in mouse CIN development and maturation using a constitutive *Cntnap2* null mouse. In conjunction, we used a transplantation method to assess cell autonomous roles for mouse *Cntnap2* in CINs. While no gross alterations were observed in the expression of several potassium channels (KV1.1, KV3.1, Kv4.2, and Kv4.3) in the null mice, there were changes in the expression of specific CIN markers and the fast-spiking CINs had altered physiology. Notably, *Cntnap2* mutant mice had reduced numbers of MGE-derived

(PV$^+$) and CGE-derived (REELIN$^+$/SST$^-$) CINs. The transplantation assay showed that *Cntnap2* is necessary to autonomously establish the number and electrophysiological properties of PV$^+$ CINs. Finally, we assessed the impact of human ASD *CNTNAP2* mutations in CIN development using a recently developed transduction/transplantation assay. We found that these human alleles were either hypomorphic or loss of function in autonomously promoting PV$^+$ CIN development.

## Materials and Methods

### Animals

*Cntnap2* knockouts (Poliak et al. 2003), Ai14 Cre-reporters (Madisen et al. 2010), and Nkx2.1-Cre (Xu et al. 2008) mouse strains have been published. Mice were initially on a mixed C57BL6/J, CD-1 background. All lines were backcrossed to CD-1 for several generations before analysis. For timed pregnancies, noon on the day of the vaginal plug was counted as embryonic Day 0.5. Animal care and procedures were performed according to the University of California at San Francisco Laboratory Animal Research Center guidelines. For single cell RNA analysis, we used the following combination of mice: chandelier cells (CHC) and PV basket cells in the cortex were labelled using the Nkx2.1-CreER (Taniguchi et al. 2013) (Tamoxifen induced at E17.5) and PV-IRES-Cre (Hippenmeyer et al. 2005) lines, which were crossed with the Ai14 reporter mouse. Intersectional labeling was achieved by breeding each of the following separately to the Ai65 intersectional reporter (Madisen et al. 2015) to label (1) Sst-Flp; Nos1-CreER for Long projecting cells (He et al. 2016), (2) Sst-Flp; CR-Cre (He et al. 2016) for Martinotti cells, (3) VIP-Flp (He et al. 2016); CR-Cre for Interneuron selective cells and (4) VIP-Flp; CCK-Cre (He et al. 2016) for Cck-basket cells. For these latter mice, the Cold Spring Harbor Laboratory animal husbandry protocol was followed (IACUC 16-13-09-8).

### Cell Counting and Statistical Analysis

For cell counts from the somatosensory cortex in constitutive mouse mutants, Image-J was used to calculate the number of CINs and then this number was divided by the area of the cortex to determine cell density. Two sections were counted from each mouse and averaged to generate each (*n*). Cell density and western blots were statistically analyzed using one-way ANOVA, followed by the Tukey's post test to determine significance. For post-hoc analysis, normality, homogeneity and independence were met. For transplanted cell counts, Image-J was also used, and those cells that were co-labeled for tdTomato and the CIN marker were counted. Since the transplanted cell data are normalized to the number of total cells transplanted, we used a nonparametric test, the Chi-squared analysis, to determine significance. For these counts, cells were assessed in multiple parts of the neocortex, due to the low number, and data were only included if at least 50 cells were counted per sample. Statistics were analyzed using Prism 6.

### DNA Vector Generation

To generate the *DlxI12b-BG-MCS-IRES-Cre* vector, the T2a site was excised from a previously reported vector (Vogt, Cho et al. 2015) and replaced with an IRES sequence. The IRES sequence was amplified from the *pIRES2-EGFP* vector (Clontech) with primers (5′ GAGATGTACAACCGGGATCCGCCCCTCT, 3′ GAGAGAA TTCTGTGGCCATATTATCATCG) that introduced BsrGI and

EcoRI sites, and then inserted into these sites in the previous vector. Next, human *CNTNAP2* cDNA (ABM) was used as a template to PCR amplify the gene with introduced 5′ XbaI and 3′ BsrGI sites, using the primers: (5′GAGATCTAGAATGCA GGCGGCTCCGCG; 3′GAGATGTACATCAAATGAGCCATTCCTT). The human *CNTNAP2* PCR fragment was cloned into these sites within the MCS of the vector. To introduce human ASD allele mutations, extension-overlap PCR was used to introduce each mutation using the following primers with introduced mutations (underlined) in combination with flanking primers (those used to amplify full length *CNTNAP2*, above): N407>S (5′ mutant GGAACCCCAGTGGTCTCCTGGTCTTCAGTCACTTTG, 3′ mutant CAGGAGACCACTGGGGTTCCATGCCTAAACTGG); N418>D (5′ mutant CTTTGCGGATGATTTGGGCAATGTGGAGATTGACCTC, 3′ mutant CATTGCCCAAATCATCCGCAAAGTGACTGAAGACCAG); G731>S (5′ mutant GTGCCTGCAGCATCGAACGCAACTGCACAGA TCCCAAG, 3′ mutant GCGTTCGATGCTGCAGGCACATTTCTGGA TTCCAGG); T1278>I (5′ mutant ATCCTGTGCATCCTGGTCTTCCT GATCCGGTACATG, 3′ mutant GAAGACCAGGATGCACAGGATGG TGAAAATCACCAC). First, 2 PCR products were generated with the primers: (5′ flanking and 3′ mutant, 5′ mutant, and 3′ flanking), using human *CNTNAP2* cDNA as a template. Next, these PCR products were combined together and PCR amplified using the *CNTNAP2* flanking primers (above) with introduced 5′ XbaI and 3′ BsrGI sites. These full length PCR products were then ligated 5′ to the *IRES* element in the XbaI and BsrGI sites of the *DlxI12b-BG-MCS-IRES-Cre* lentiviral vector. All vectors were verified by sequencing.

## Electrophysiology

Slice preparation and intracellular recordings followed our published protocol (Sohal and Huguenard 2005). Coronal slices, 250 μm thick, from mice of either sex were cut in a chilled slicing solution in which Na$^+$ was replaced by sucrose, then incubated in warmed ACSF at 30–31 °C for 15 min and then at least one hour at room temperature before being used for recordings. ACSF contained (in mM): 123 NaCl, 26 NaHCO₃, 3 KCl, 1.25 NaH₂PO₄, 1 MgCl₂, 2 CaCl, and 11 glucose. Slices were secured by placing a harp along the midline between the 2 hemispheres.

### Intracellular Recordings

Somatic whole-cell patch recordings were obtained from tdTomato$^+$ CINs in somatosensory cortex on an upright microscope (BX51WI; Olympus). Recordings were made using a Multiclamp 700A (Molecular Devices). Patch electrodes (tip resistance = 2–6 MΩ) were filled with the following (in mM): 130 K-gluconate, 10 KCl, 10 HEPES, 10 EGTA, 2 MgCl₂, 2 MgATP, and 0.3 NaGTP (pH adjusted to 7.3 with KOH). All recordings were at 32.5 ± 1 °C. Series resistance was usually 10–20 MΩ, and experiments were discontinued above 30 MΩ.

### Analysis of intrinsic properties

Intrinsic properties were calculated based on the current-clamp responses to a series of 250msec current pulse injections from −200 to 450 pA (50 pA/increment). Input resistance was calculated from the voltage response to a −50 pA, 250 ms current pulse. Spiking properties were calculated based on the response to a current pulse that was 100 pA above the minimal level that elicited spiking. Recorded CINs were therefore subdivided into fast-spiking (FS) or non-FS based on electrophysiological properties. Since fast-spiking PV$^+$ CINs have minimal spike adaptation and lower input resistances compared to SST$^+$ CINs (Kawaguchi 1993; Kawaguchi and Kubota 1996), cells were separated into accommodating and nonaccommodating cells based on adaptation ratio and input resistance. Specifically, we classified a CIN as fast-spiking if the adaptation ratio was <1.3, and the input resistance was <350 MΩ. All data show means ± SEM and are analyzed using 2-tailed Student's unpaired *t*-tests.

## HEK293T Cell Cultures

HEK293T cells were maintained in DMEM supplemented with 10% fetal bovine serum. For analysis of the human CNTNAP2 expression vectors, the vectors were transfected into HEK293T cells using Lipofectamine$^{2000}$ (ThermoFisher). After 48 h, the cells were fixed with 4% paraformaldehyde (PFA) and immunelabeled with a rabbit anti-CASPR2 (Millipore) antibody. The appropriate Alexa-conjugated secondary was used to detect CASPR2$^+$ cells and DAPI was used to detect cell nuclei. Lentiviral production using HEK293T cells were performed as previously described (Vogt, Wu et al. 2015).

## Immunofluorescence tissue staining

Either P30 *Cntnap2* constitutive KO mice and controls, or P35 MGE-transplanted mice, were transcardially perfused, first with phosphate-buffered saline, followed by 4% PFA. After perfusion, brains were removed and postfixed in PFA for 30 min, then sunk in 30% sucrose overnight before embedding in OCT and freezing. About 25 μm coronal brain sections were made using a cryostat. Immunofluorescence labeling was performed on these cryosections with the following primary antibodies: rabbit anti-parvalbumin (Swant), rat anti-somatostatin (Millipore), rabbit anti-VIP (Immunostar), mouse anti-Reelin (Millipore). The appropriate 488, 594, or 647 Alexa-conjugated secondary antibodies were from Life Technologies. Sections were cover slipped with Vectashield containing DAPI (Vector labs).

## MGE Transplantation

MGE transplantations were done as described (Vogt, Wu et al. 2015). Briefly, E13.5 MGE tissue from either *Cntnap2$^{+/−}$* or *Cntnap2$^{−/−}$* embryos were dissociated, then transduced with lentiviruses for 30 min. Next, the cells were washed to remove excess virus, pelleted and then transplanted into the cortices of WT P1 host mice. The cells developed for 35 days in vivo, and were then assessed via native tdTomato fluorescence.

## Lentiviral Production

Lentiviral production was performed as previously described (Vogt, Wu et al. 2015). Briefly, HEK293T cells were transfected using Lipofectamine2000 (Invitrogen) with 4 plasmids to generate lentivirus particles as previously described, including the lentiviral expression vector, *pVSV-g*, *pRSVr*, and *pMDLg-pRRE*. Media containing virus was collected and ultracentrifuged at 100 000 × g for 2.5 h at 4 °C. After the ultracentrifuge step, supernatant was removed and the pellet was resuspended in sterile PBS then stored at −80 °C until use.

## Single Cell RNA Analysis

### Manual Cell Sorting

Single cells were collected from P28–35 animals by manual sorting procedure as previously described (Paul et al. 2012). Brains were sectioned at 300 μm thickness, micro-dissected, and dissociated. Single RFP-positive cells were collected using patch pipette capillary and dispensed individually into separate

single tubes prefilled with RNAseOUT (Invitrogen), ERCC spike-in RNAs in 1:400 K dilution, sample specific RT primers. Process was repeated to collect 32–64 cells in one manual cell sorting session. Cells were flash frozen in liquid nitrogen and stored at −80 °C until processed. Patch pipette was single use only and fresh pipettes were used for every single cell collected.

*Linear RNA Amplification, Illumina Library Prep, and Sequencing*
RNA was linearly amplified by T7 RNA polymerase using 2 rounds of in vitro transcription (MessageAmp-II kit Life Technologies) according to the manufacturer's recommended protocol with some modifications to make aRNA. Second round aRNAs were fragmented chemically using NEBNext® Magnesium RNA Fragmentation Module (Cat#E6150S), column purified using RNA MinElute (Qiagen) for final Illumina cDNA library preparation steps using Illumina TruSeq small RNA kit (Cat#RS-200-0012) (Hashimshony et al. 2012). The resulting library was paired-end sequenced for 101 bp in Illumina HiSeq.

*Mapping and Tag Counting*
Bowtie was used for sequence alignment of read2 (polyA primed) to the mouse reference genome (mm9), and read1 sequences were used for UMI (varietal-tag) counting. Using a custom python script (https://github.com/maggiecrow/scCoexp), multiple reads to the same gene with the same tag sequences were rejected and only counted as one, such that only mapped sequences with unique tags were retained and tallied for each mRNA for each cell.

## Western Blotting

E13.5 MGE tissue was dissected and lysed in RIPA buffer (150 mM NaCl, 1% NP-40, 0.1% SDS, 0.5% sodium deoxycholate in 50 mM Tris) supplemented with protease (Halt protease inhibitor, Pierce) and phosphatase (PhosSTOP, Roche) inhibitors. ~20 μg of total protein was loaded into an SDS-PAGE gel, separated, and transferred to a nitrocellulose membrane. The membrane was probed with the following antibodies: rabbit
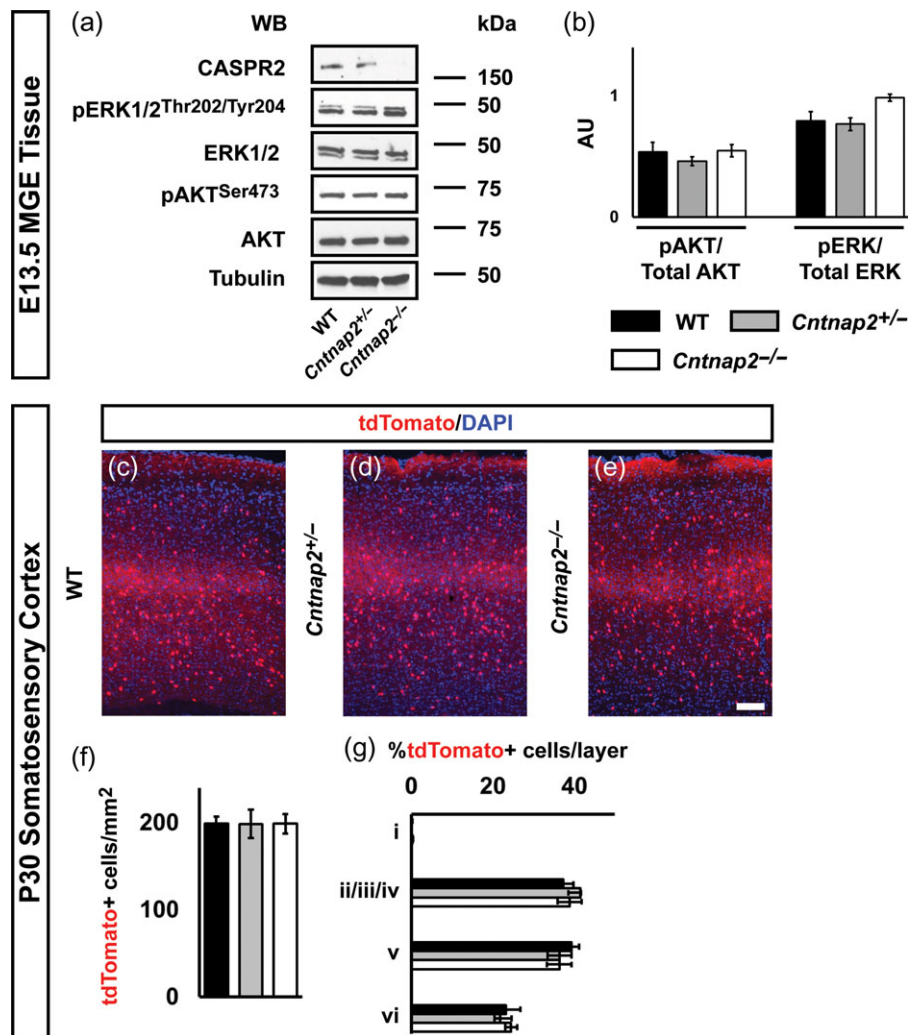


**Figure 1.** *Cntnap2$^{-/-}$* mice exhibit an increased trend for pERK1/2 in embryonic MGE but no gross changes in MGE-derived CIN numbers or lamination. Western blots from E13.5 MGE tissue lysates showing CASPR2, pERK1/2$^{Thr202/Tyr204}$, total ERK1/2, pAKT$^{Ser473}$, total AKT, and βIII-tubulin (loading control) (*a*). (*b*) quantification of the levels of pAKT or pERK divided by the total amount of AKT or ERK expressed as arbitrary units (AU). (*c*–*e*) Immunofluorescence images in coronal sections showing MGE-derived CINs, tdTomato$^+$ and co-labeled with DAPI, in the somatosensory cortex at P30. (*f*) Quantification of tdTomato$^+$ cell density in the somatosensory cortex at P30. (*g*) Quantification of the proportion of tdTomato$^+$ cells per lamina at P30. Data are expressed as mean ± SEM. *n* = 3, all groups. Scale bar in (*e*) = 100 μm.

anti-CASPR2 (Millipore), rabbit anti-pAKT[Ser473] (Cell Signaling), rabbit anti-total AKT (Cell Signaling), pERK1/2[threonine 202/tyrosine 204] (Cell Signaling), total ERK1/2 (Cell Signaling), mouse anti-βIII-tubulin (Covance), and the species-appropriate HRP-conjugated secondary antibodies (Biorad). HEK293T cells were transfected with human CNTNAP2 expression vectors using Lipofectamine[2000] (ThermoFisher), and cell lysates were collected after 48 h in the same manner described above. The rabbit anti-CASPR2 (Millipore), rabbit anti-GFP (ThermoFisher) and appropriate HRP-conjugated antibodies (BioRad) were used to detect proteins.

## Results

### Cntnap2 Constitutive Mutants have Normal Numbers of CINs in the Nkx2-1 Lineage, but Decreased PV and Reelin Expression

Towards obtaining a deeper understanding of the role of *Cntnap2* in CIN development and function, we first studied the constitutive null mutant (Poliak et al. 2003). We concentrated on CINs derived from the medial ganglionic eminence (MGE). Thus, we began by assaying CASPR2 protein expression in embryonic day (E) 13.5 MGE tissue from WT, *Cntnap2^{+/−}*, and *Cntnap2^{−/−}* using western blotting. We found that CASPR2 was expressed in the MGE at this age, and its expression was not detectable in *Cntnap2^{−/−}* MGE tissue (Fig. 1a).

Little is known about whether the CASPR2 protein regulates intracellular signaling. Thus, we compared various signaling pathways from WT, *Cntnap2^{+/−}*, and *Cntnap2^{−/−}* in E13.5 MGE tissue. We focused on signaling pathways that are implicated in some subtypes of ASD: MAPK and PI3K/AKT/mTOR pathways (Chen et al. 2014; Wen et al. 2016). We assayed the levels of ERK1/2 and AKT proteins as well as phosphorylated epitopes of these proteins that are indicative of increased activity: pAKT[serine 473], pERK1/2[threonine 202/tyrosine 204]. While there was an increased trend for pERK1/2[threonine 202/tyrosine 204] (Fig. 1a), these levels were not significantly different than WTs (Fig. 1b). We also found no change in pAKT[serine 473]. Due to the increased trend in pERK embryonically, we explored whether *Cntnap2^{−/−}* mice had a change in MGE

proliferation (at E13.5 and E15.5) and cell survival at postnatal day (P) 0 and P7, but did not observe any changes (data not shown).

Since earlier reports have shown decreased numbers of GABAergic neurons and/or decreased CIN subgroups after *Cntnap2* deletion (Peñagarikano et al. 2011; Hoffman et al. 2016), we assessed numbers of CINs and the different CINs subgroups in adult mouse brains at P30. Our primary goal was to understand if the number of CINs derived from the MGE and Preoptic Area (POA) were altered in *Cntnap2^{−/−}* mice, since these population comprise ~70% of all CINs. To this end, we crossed the *Nkx2.1-Cre* allele (Xu et al. 2008) into mice that had the *Cntnap2* null allele. In addition, the Cre-dependent reporter, *Ai14* (Madisen et al. 2010), was also utilized to follow tdTomato[+] (red fluorescence) MGE and POA-derived cells. Notably, loss of *Cntnap2* did not change the number of tdTomato[+] CINs in the P30 somatosensory cortex (Fig. 1c–f), or their laminar distribution at this age (Fig. 1g). Finally, we examined the number of MGE and POA-derived cells in the striatum, and pallidum but found no differences (data not shown). Overall, these results suggest that *Cntnap2^{−/−}* mice generate and maintain normal numbers of MGE and POA-derived CINs by P30.

While *Cntnap2* is expressed in MGE tissue (Fig. 1), it is unknown whether it is also expressed in postnatal CINs. To assess this, we performed single cell RNA sequencing from known Cre-driver lines to assess the level of *Cntnap2* transcript in cells from P28–P35 as previously described (Paul et al. in press). *Nkx2.1-CreER* and *PV-IRES-Cre* crossed to *Ai14* reporter mice were used to isolate adult chandelier cells (CHC) and PV^{+} cells, respectively. These cells had high levels of *Cntnap2* transcripts in the adult cortex compared with other CIN subtypes (Fig. 2a,b). Next, we used a combination of *Sst-Flp* and *Nos1-CreER* lines to isolate SST[+] long projecting cells or *Sst-Flp* with the calretinin (CR)-Cre to label SST^{+} Martinotti cells. While there was *Cntnap2* transcript in these populations (Fig. 2a,b), it was lower than in the CHC and PV lineage groups. Finally, we examined CGE-derived VIP[+] CINs by utilizing a combination of the *VIP-Flp* with *CR-Cre* to isolate interneurons or the *VIP-Flp* with *CCK-Cre* to label CCK^{+} basket cells. Each of these VIP[+] groups also had high levels of *Cntnap2* transcript (Fig. 2a,b). Overall, many CINs express *Cntnap2* in the postnatal cortex, with higher levels of expression in the CHC/PV[+] and VIP[+] subgroups and lower expression in the SST[+] subgroups. Due to a lack of Cre-driver lines to specifically isolate the REELIN[+]; SST[−] CINs derived from the CGE, we do not know if *Cntnap2* is expressed in these cells postnatally.

Next, we assessed whether distinct groups of CINs were affected in *Cntnap2* mutants. To this end, we first examined parvalbumin (PV)[+] and somatostatin (SST)[+] CINs; the main CINs derived from the MGE. There was ~24% decrease in PV-expressing CINs in *Cntnap2^{−/−}* cortices (Fig. 3a–d, P = 0.006), similar to a previous report (Peñagarikano et al. 2011). We found no change in SST[+] CINs (Fig. 3e–h).

We then investigated CGE-derived CINs, including those expressing vasoactive intestinal peptide (VIP) or REELIN (but that do not express SST) (Wonders and Anderson 2006; Miyoshi et al. 2010). Notably, there was ~13% decrease in REELIN[+]/SST[−] CINs (Fig. 3e–g,i, P = 0.049). However, no differences in VIP[+] CINs were evident (Fig. 3j–m). Thus, specific subgroups of both MGE and CGE-derived CINs were reduced in *Cntnap2^{−/−}* mutants.

### Cell Autonomous Role of CNTNAP2 in Mediating Cell Intrinsic Properties of PV[+] Fast-Spiking CINs

It is unknown whether *Cntnap2* loss of function alters the molecular and/or physiological properties of CINs via cell
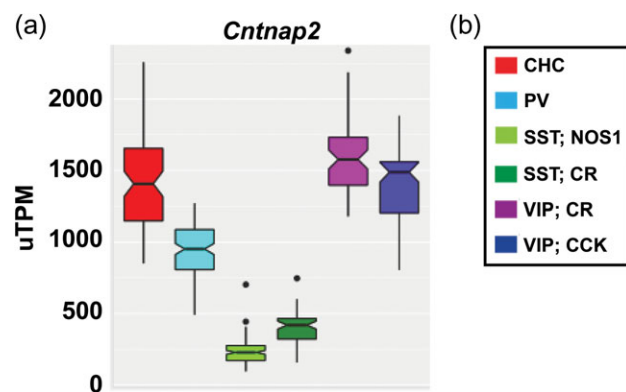


**Figure 2.** *Cntnap2* expression in different CIN subgroups. Transcript levels of *Cntnap2* from purified single GABAergic neurons from adult mouse cortices using distinct Cre-driver lines (see methods for details). (a) Box plots showing quantification of the unique transcripts per million (uTPM) for Cntnap2. Single CHC and PV[+] CINs as well as VIP[+] CINs (both CR[+] and CCK[+]) have high levels of *Cntnap2* in the adult cortex. While SST[+] CINs (both Nos1^{+} and CR[+]) express *Cntnap2*, the number of unique transcripts per million is lower than the previous groups. Single black dots in (a) represent outlier values. (b) Legend to denote the types of single cells assessed. CHC, Chandelier Cell; CR, calretinin; CCK, cholecystokinin; Nos, Nitric Oxide Synthase.
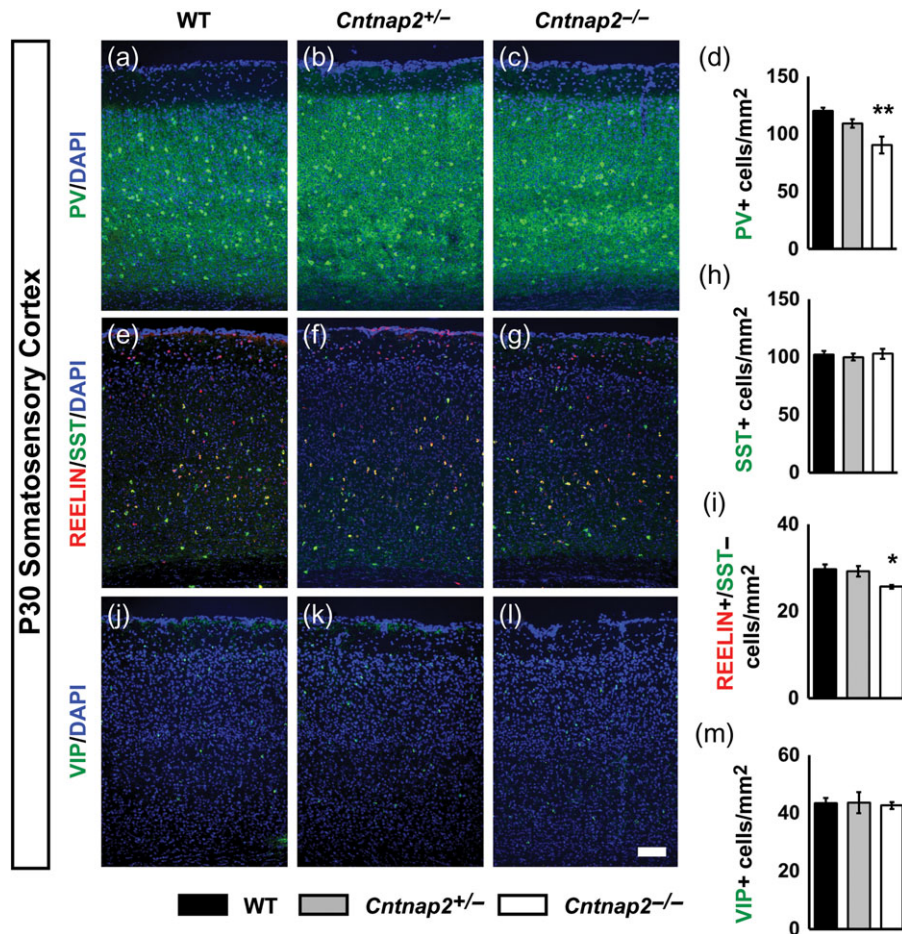
**Figure 3.** *Cntnap2* constitutive null mice have decreased numbers of the CIN markers PV and REELIN in the somatosensory cortex. Immuno-fluorescent images from the somatosensory cortex of P30 WT (*a, e, j*), *Cntnap2*+/− (*b, f, k*), or *Cntnap2*−/− (*c, g, l*) mice. Images show both MGE-derived (PV+ and SST+) and CGE-derived (VIP+ and REELIN+/SST−) CINs co-stained with DAPI. Quantification of the cell density of PV+ (*d*), SST+ cells (*h*) or REELIN+/SST− (*i*) or VIP+ (*m*) cells in the somatosensory cortex at P30. Data are represented as mean ± SEM. $n = 3$, all groups. Scale bar in (*l*) = 100 μm. *$P < 0.05$, **$P < 0.01$.

autonomous mechanisms, and/or by secondary defects induced by other cells. A *Cntnap2* conditional mouse could help solve this problem, however, this mouse does not currently exist to our knowledge. To overcome this roadblock, we employed an MGE cell transplantation approach (Vogt, Wu et al. 2015), in which E13.5 *Cntnap2*−/− MGEs (containing immature CINs) are transplanted into the normal environment of a P1 WT cortex, where they develop and mature *in vivo*. We fluorescently labeled WT, *Cntnap2*+/−, and *Cntnap2*−/− MGE cells with tdTomato expression, by including the *Nkx2.1-Cre* and *Ai14* alleles, and assessed their electrophysiological properties at 6–8 weeks post transplantation (see schema, Fig. 4*a*).

The transplanted tdTomato+ CINs were separated into 2 subgroups based on their spike responses to depolarizing current pulses: accommodating (non fast-spiking, likely SST+ CINs) or nonaccommodating (fast-spiking, likely PV+ CINs) (see Materials and Methods section). Notably, the nonaccommodating, presumed PV+, CINs had multiple parameters that were changed in *Cntnap2*−/− mutants. Based on their responses to a series of current injections, the nonaccommodating interneurons lacking *Cntnap2* displayed wider spikes, smaller maximum rate of rise of membrane voltage during spike rising phase, slower membrane time constants, greater adaptation ratios, and more depolarized resting membrane potentials compared to controls (Fig. 4*b–f*, WT compared to null: half-width $P = 0.002$, max slope $P = 0.002$, tau

$P = 0.02$, ISI $P = 0.01$). Example traces for nonaccommodating CINs are shown in Figure 4*i*. These changes suggest a role for *Cntnap2* in the properties of voltage-dependent sodium and/or potassium and/or sodium channels, which mediate action potentials and repolarization in nonaccommodating CINs. Interestingly, in *Cntnap2* heterozygote CINs several of these properties had values intermediate between those of the WT and *Cntnap2* null CINs. While one (action potential half-width) was significantly different between the heterozygotes and nulls (Fig. 4*b*, $P = 0.02$), there were other parameters for which both heterozygotes and knockouts were significantly different compared to WTs (Fig. 4*h*, *f-I* slope, (heterozygote $P = <0.0001$, null $P < 0.0001$). Thus, loss of one *Cntnap2* allele is sufficient to elicit physiological changes in nonaccommodating, presumed PV+, CINs.

In contrast, the accommodating (likely SST+) *Cntnap2* null CINs did not show differences in the same cell intrinsic properties (Fig. 4*j–p*). Together, our data provide evidence that *Cntnap2* preferentially regulates the physiological properties of presumed PV+, fast-spiking CINs.

## Cell Autonomous Role for Human ASD CNTNAP2 Alleles in Regulating the Number of CINs that Express PV

To probe the functional consequences of missense mutations discovered in *CNTNAP2*, we cloned the WT human *CNTNAP2*
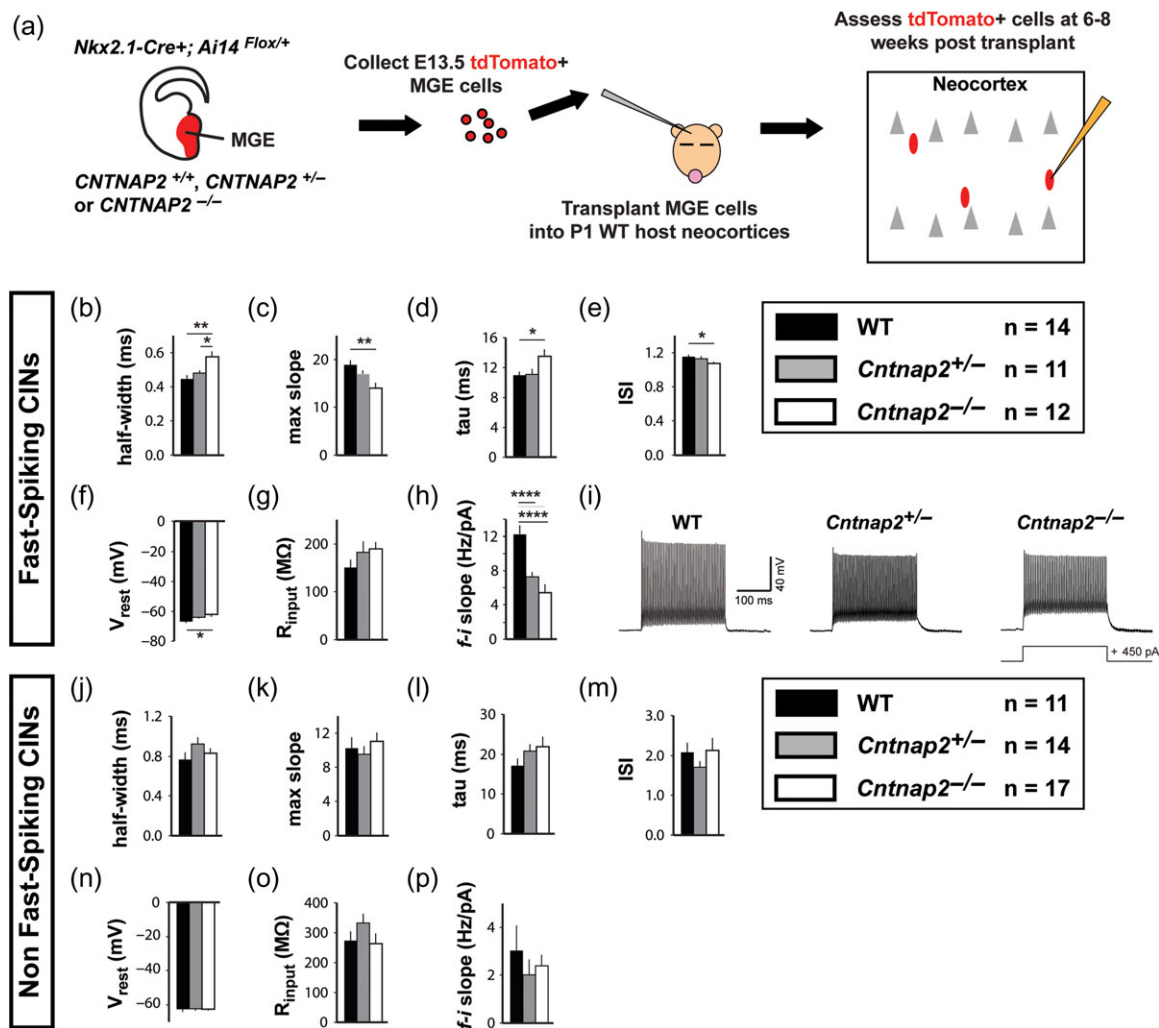
**Figure 4.** *Cntnap2* MGE-derived CINs show cell autonomous alterations selectively in PV$^+$ cell intrinsic properties. Schema depicting MGE cell transplantation and electrophysiological analysis (a). Briefly, E13.5 MGE cells were dissected from *Nkx2.1-Cre$^+$*; *Ai14$^{Flox/+}$* embryos that were either WT, *Cntnap2$^{+/-}$* or *Cntnap2$^{-/-}$*, then dissociated and injected into the cortices of WT P1 host mice. The cells developed *in vivo* until 6–8 weeks post-transplant and the tdTomato$^+$ cells were assessed. The cells were grouped into either non-accommodating (b–h) or accommodating (j–p). The action potential half-width, maximum slope, membrane time constant (tau), adaptation ratio (inter spike interval, ISI), resting membrane potential (Vrest), resting input resistance (Rinput), and f-I slope were calculated from current-clamp responses of the tdTomato$^+$ CINs to brief current pulses (−50 pA for input resistance, 100 pA above spiking threshold for other parameters). (i) Example current-clamp responses of transplanted, tdTomato$^+$ non-accommodating (fast-spiking) CINs to injection of depolarizing current in WT (left), *Cntnap2$^{+/-}$* (middle), and *Cntnap2$^{-/-}$* (right) mice. Data are represented as mean ± SEM. *$P < 0.05$, **$P < 0.01$, ****$P < 0.0001$.

gene, as well as 4 reported *CNTNAP2* missense alleles discovered in individuals diagnosed with ASD (Bakkaloglu et al. 2008), into a *DlxI12b-IRES-Cre* lentiviral vector before the *IRES* sequence and the *Cre*-recombinase gene (Fig. 5a). *DlxI12b* is an enhancer that is preferentially expressed in GABAergic neurons (Potter et al. 2009; Arguello et al. 2013). We chose to investigate 4 missense *CNTNAP2* alleles discovered in populations with ASD (Bakkaloglu et al. 2008), as little is known about whether these missense alleles alter *CNTNAP2* function. Expression of each of the *CNTNAP2* alleles was verified by western blotting following transfection of the vector into HEK293T cells (Fig. 5b). We also verified the Cre activity from each vector by its ability to induce expression of GFP from a Cre-dependent GFP-expression plasmid (Fig. 5b). Finally, we expressed the WT and mutant CNTNAP2 alleles in HEK293T cells and found that both the WT and mutant proteins were enriched at cell membranes (Fig. 5c–h).

Next, we used a modification of the MGE transplantation assay (Vogt, Wu et al. 2015) to study the functional properties

of human *CNTNAP2* mutant alleles on CINs. To this end, MGE cells from *Cntnap2$^{+/-}$* or $^{-/-}$ E13.5 mouse embryos were dissociated and transduced with the *DlxI12b-IRES-Cre* lentivirus (schema, Fig. 5a), before being transplanted into the cortices of P1 WT pups. The MGE cells also harbor the *Ai14* allele, to visualize tdTomato after Cre recombination in the transduced cells.

Virus encoding either the "empty" vector (Cre only), or a virus encoding one of the human *CNTNAP2* alleles and *Cre* were transduced into mouse E13.5 *Cntnap2$^{-/-}$* or *Cntnap2$^{+/-}$* MGE cells before transplantation and assessed for PV expression at 35 days post-transplant (DPT). Notably, *Cntnap2$^{-/-}$* transplanted MGE cells had ~33% reduction in PV$^+$ CINs compared with *Cntnap2$^{+/-}$* transplants (Fig. 6h,o), demonstrating that reduced PV$^+$ CINs is a cell autonomous phenotype. Of note, WT human *CNTNAP2*, transduced into *Cntnap2$^{-/-}$* MGE cells, completely rescued the number of PV-expressing cells (Fig. 6b,c,h, $P = 0.004$). However, transduction of human *CNTNAP2* into heterozygous *Cntnap2* cells did not alter the number of PV-expressing
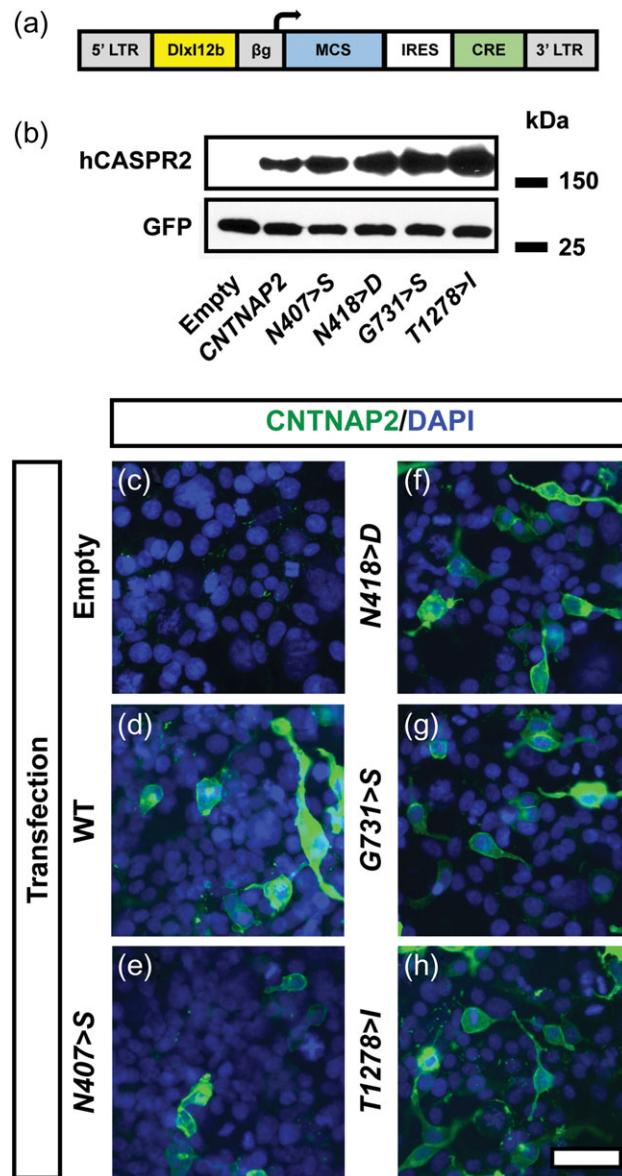
**Figure 5.** Human *CNTNAP2* allele expression and a lentiviral expression vector for transduction. Schema of a lentiviral expression vector to express Cre and human *CNTNAP2* alleles, cloned into the MCS (*a*). (*b*) Western blots showing expression of human *CNTNAP2* alleles and GFP from a Cre-dependent GFP-expression vector in HEK293T cells. (*c–h*) Immuno-fluorescent images of HEK293T cells that were transfected with either an empty version of the vector shown in (*a*) or vectors containing WT or mutant human *CNTNAP2* alleles. Cells expressing CASPR2 show that both the WT and mutant proteins are detected at the cell membrane. Abbreviations: LTR, DlxI12b, βg, MCS, IRES. Scale bar in (*h*) = 250 μm.

cells (Fig. 6*i,j,o*). Thus, human *CNTNAP2* complemented the decreased PV$^+$ interneuron phenotype in mouse MGE cells that lacked the gene but did not act in a dominant fashion in the heterozygous cells.

Next, we tested whether the 4 human *CNTNAP2* missense mutations, could rescue the reduction in PV$^+$ CINs in the transplanted *Cntnap2$^{-/-}$* MGE cells. None of the mutant alleles showed a significant rescue of PV$^+$ CIN numbers and were significantly different than WT *CNTNAP2* transduction (Fig. 6*d–h*, N407>S $P < 0.0001$; N418>D $P = 0.006$; G731>S $P = 0.0003$; T1278>I $P = 0.007$, compared to WT *CNTNAP2* transduction). To explore if the mutant alleles act in a dominant-interfering fashion, we transduced them into heterozygote (*Cntnap2$^{+/-}$*) MGE cells. Only G731>S showed a trend towards reduced PV$^+$ CINs in *Cntnap2$^{+/-}$* CINs, but this effect did not reach statistical

significance (Fig. 6*i–o*, G731>S $P = 0.31$). We also examined SST$^+$ CINs in these assays, but did not observe any differences between groups (data not shown). In sum, 4 human *CNTNAP2* missense mutations acted like null/hypomorphic alleles based on their inability to rescue the number of PV$^+$ CINs.

We also explored whether transplanted MGE cells lacking *Cntnap2* or those transduced with human *CNTNAP2* alleles mutated in ASD resulted in elevated ERK1/2 activity but found no changes in adult brains (data not shown), suggesting that this may be a transient phenotype.

## Discussion

Herein, we focused on cell autonomous roles for *CNTNAP2* in CIN development and physiology. As described previously, we found
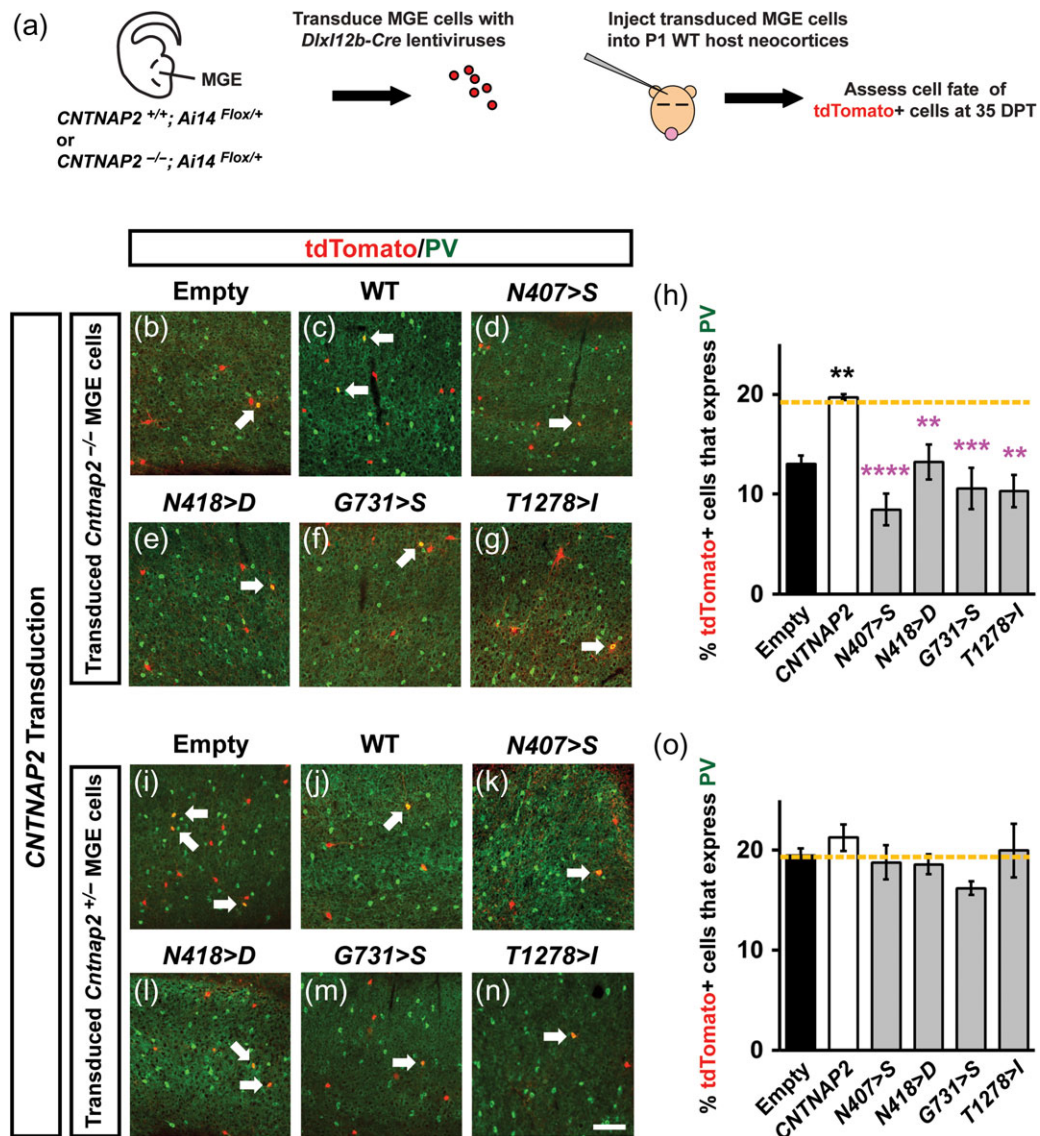
**Figure 6.** Human ASD *CNTNAP2* mutants fail to complement the mouse *Cntnap2$^{-/-}$* PV$^+$ phenotype *in vivo*. Schema depicting an assay to screen the function of human mutant alleles *in vivo* within developing/maturing CINs (*a*). E13.5 MGE cells from *Cntnap2$^{-/-}$*; *Ai14$^{Flox/+}$* mouse embryos were transduced with viruses expressing Cre only (Empty) or that also expressed human *CNTNAP2* alleles. The transduced cells were transplanted into WT mouse host neocortices and developed until 35 DPT. (*b–g* and *i–n*) Immuno-fluorescent images of transplanted cells, tdTomato$^+$, in the neocortex that were co-labeled for PV. Arrows point to co-expressing cells. Quantification of the proportion of *Cntnap2$^{-/-}$* (*h*) or *Cntnap2$^{+/-}$* (*o*) transduced-MGE cells that co-express PV. Yellow dotted lines represent control levels of PV$^+$ cells. Data are represented as mean ± SEM. *n* = 3–4, all groups, (**P < 0.01, ***P < 0.001, ****P < 0.0001). Scale bar in (*n*) = 100 μm.

that *Cntnap2$^{-/-}$* mice had reduced numbers of PV$^+$ MGE-derived CINs (Peñagarikano et al. 2011). We extended this analysis in many ways (see below), including by demonstrating that *Cntnap2$^{-/-}$* mice also had reduced numbers of REELIN$^+$/SST$^-$ (CGE-derived) CINs. We also showed the specificity of this phenotype as the number of other MGE (SST$^+$) and CGE (VIP$^+$)-derived CINs were normal.

We provided evidence that the reduction of PV$^+$ CINs was not due to a reduction in the number MGE-derived CINs by using *Nkx2-1-Cre*-fate mapping (Fig. 1). This suggests that the reduction in PV$^+$ CINs was not due to a defect in their production, migration, and/or survival, but probably due to a defect in their differentiation and/or activity, that secondarily reduced expression of the PV protein. Indeed, PV expression in CINs does not begin until ~P10–P14, which may depend, at least in part, on neural activity

(Vogt Weisenhorn et al. 1998; Patz et al. 2004). While we did not detect a decrease in MGE-derived CINs, it should be noted that others have noted a reduction in GABAergic cells in zebrafish that have *Cntnap2* deletion (Hoffman et al. 2016). The discrepancies between our findings could be due to several mechanisms, such as species differences or experimental approaches. Fate mapping in the mouse *CNTNAP2* mutant using a Cre that is active in all/most CINs (e.g., *GAD2-Cre*) could help resolve the issue of whether there is a global reduction of cortical CINs.

Importantly, our MGE transplantation experiments showed that *Cntnap2$^{-/-}$* CINs, which had differentiated in a WT cortex, also generated fewer CINs that were PV$^+$ (Fig. 6). This provides evidence that *Cntnap2* is autonomously required during CIN maturation to promote PV expression, perhaps because of abnormal activity within these cells.

*Cntnap2*$^{-/-}$ MGE-derived CINs had multiple abnormal cell intrinsic physiological properties (Fig. 4). The results provide evidence that *Cntnap2* is particularly important in PV$^+$, nonaccommodating, fast-spiking CINs, rather than in accommodating/likely SST$^+$ CINs. Consistent with this, *Cntnap2* RNA is more highly expressed in PV$^+$ fast-spiking CINs than in SST$^+$ CINs (Fig. 2). Interestingly, in the constitutive *Cntnap4* loss of function mouse, the action potential width in PV$^+$ CINs was significantly increased (Karayannis et al. 2014), similar to our observations in transplanted *Cntnap2*$^{-/-}$ fast-spiking CINs (Fig. 4). Moreover, while other cell intrinsic properties (i.e., input resistance, tau, and firing rate) in the constitutive *Cntnap4* mutant did not reach significance, changes in their values trended in the same direction as the changes we found in the *Cntnap2*$^{-/-}$ fast-spiking CINs. These data suggest these 2 neurexin family members have some overlapping functions in fast-spiking CINs.

The changes in half-width, maximum slope, resting membrane potential, and adaptation ratio suggest that the *Cntnap2*$^{-/-}$ fast-spiking CINs could have alterations in potassium and/or sodium channels that are associated with the fast-spiking/nonaccommodating electrophysiological phenotype. CASPR2 is known to co-localize with Kv1.1 and Kv1.2 potassium channels (Poliak et al. 1999). However, our analyses of Kv1.1, Kv3.1, Kv4.2, and Kv4.3 expression, and their intracellular localization, did not reveal differences between WT and *Cntnap2*$^{-/-}$ CINs (data not shown).

*Cntnap2*$^{+/-}$ transplanted CINs exhibited intermediate phenotypes between transplanted WT and *Cntnap2*$^{-/-}$ CINs (Fig. 4). Thus, the demonstration that *Cntnap2*$^{+/-}$ heterozygote CINs have electrophysiological alterations in PV$^+$ CINs may be clinically relevant as some individuals have heterozygous mutations in *CNTNAP2*. Finally, while physiological parameters were altered in the mouse *Cntnap2*$^{+/-}$ heterozygous CINs, CIN numbers and molecular CIN markers were only altered in *Cntnap2*$^{-/-}$ nulls, suggesting that CIN physiological parameters may be more sensitive to the *Cntnap2*-heterozygous state. This is interesting in relation to humans that harbor *CNTNAP2* mutations, as they can exist in both the heterozygous or homozygous state. We hypothesize that individuals with heterozygous mutations may potentially have alterations in the physiological properties of PV$^+$ CINs but may lack more severe phenotypes associated with complete loss of functional *CNTNAP2*. Of note, individuals that have homozygous mutations that result in nonfunctional protein exhibit severe phenotypes including epilepsy, speech and language impairment as well as intellectual disability (Strauss et al. 2006; Zweier et al. 2009; Watson et al. 2014; Rodenas-Caudrado et al. 2016).

Human *CNTNAP2* disease alleles have been discovered in individuals with ASD and other neurological disorders. It is important to interrogate *CNTNAP2* function encoded by these alleles using relevant assays, particularly in vivo. Herein, we focused on a subset of *CNTNAP2* missense alleles reported in ASD individuals (Bakkaloglu et al. 2008).

Previously, we validated an efficient in vivo approach to determine the impact of ASD alleles; we first applied this to *PTEN* (Vogt, Cho et al. 2015). Here, we utilized this approach to evaluate the function of *CNTNAP2* ASD mutations in MGE-derived CINs that did not express mouse *Cntnap2*. Notably, none of the mutant human *CNTNAP2* alleles could rescue the reduction of PV$^+$ CINs. In addition, none of them induced phenotypes when expressed in *Cntnap2*$^{+/-}$ cells, providing evidence that they did not have a dominant effect. Together, these data provide evidence that these mutant alleles are either hypofunctional or loss of function, with respect to promoting the development of PV$^+$ CINs. Furthermore, our results support a

functional consequence of these human missense mutations on human CIN development. Likewise, we previously found *PTEN* ASD missense alleles to be hypo/loss of function but not dominant-interfering (Vogt, Cho et al. 2015).

Many ASD mouse models have alterations in PV$^+$ CINs (Selby et al. 2007; Gogolla et al. 2009; Martins et al. 2011; Takano 2015), suggesting that dysfunction or alterations in this cell type is a common lesion found in ASD. While we currently do not understand why all 4 *CNTNAP2* missense alleles resulted in decreased CINs expressing PV, PV expression is a late event in the development of these CINs and any number of developmental insults may contribute to this phenotype. Thus, our defining a role for *CNTNAP2* in PV$^+$ CIN development and maturation elucidates a mechanism that may be part of a common pathway that leads to cortex dysfunction in some forms of ASD, and potentially in other disorders caused by *CNTNAP2*. We propose that our findings have implications for understanding how *CNTNAP2* disease alleles result in specific phenotypes in ASD, perhaps through reducing cortical inhibition and thereby disrupting the E/I balance (Rubenstein and Merzenich 2003; Sudhof et al. 2009). Future studies are needed to understand if mutations in *CNTNAP2* associated with the wider spectrum of *CNTNAP2* disorders (Rodenas-Cuadrado et al. 2014; Poot 2015, 2017) have similar phenotypes.

We also detected trends towards increased pERK1/2 activity in *Cntnap2*$^{-/-}$ MGE tissue (Fig. 1*a*) that should be examined in future studies. Disruptions in RAS/MAPK signaling cause multiple disorders (known as RASopathies) that have a high comorbidity with ASD (Adviento et al. 2014). Thus, it is possible that human *CNTNAP2* may regulate MAPK signaling. At this point, we do not know whether the increased pERK1/2 activity contributes to the decreased number of PV$^+$ and REELIN$^+$/SST$^-$ CINs, and/or to the alterations in intrinsic electrophysiological properties. However, it is intriguing that ERK1/2 can target potassium channels (Schrader et al. 2006, 2009), which could explain the altered electrophysiological properties found in the fast-spiking CINs.

In sum, our results provide new insights into the cell autonomous functions of *CNTNAP2* in the development and physiology of CINs. They highlight *CNTNAP2*'s function in PV$^+$ CINs, a cell type whose dysfunction may have a central role in ASD as well as other neurological disorders.

## Authors' Contributions

D.V., K.K.A.C., S.M.S., and A.P. performed experiments and analyzed data. A.P. and J.H. contributed the single cell adult CIN RNA-seq data. All authors contributed to writing the manuscript.

## Funding

## Notes

We would like to thank Ruoqi Gao (Peter Penzes lab, Northwestern University) for helpful discussions concerning CASPR2 antibodies. *Conflict of interest statements*: J.L.R.R. is cofounder, stockholder, and currently on the scientific board of *Neurona*, a company studying the potential therapeutic use of interneuron transplantation. All other authors have no disclosures.

# References

Adviento B, Corbin IL, Widjaja F, Desachy G, Enrique N, Rosser T, Risi S, Marco EJ, Hendren RL, Bearden CE, et al. 2014. Autism traits in the RASopathies. J Med Genet. 51:10–20.

Alarcon M, Abrahams BS, Stone JL, Duvall JA, Perederiy JV, Bomar JM, Sebat J, Wigler M, Martin CL, Ledbetter DH, et al. 2008. Linkage, association, and gene-expression analyses identify CNTNAP2 as an autism-susceptibility gene. Am J Hum Genet. 82:150–159.

Anderson GR, Galfin T, Xu W, Aoto J, Malenka RC, Südhof TC. 2012. Candidate autism gene screen identifies critical role for cell-adhesion molecule CASPR2 in dendritic arborization and spine development. Proc Natl Acad Sci USA. 109: 18120–18125.

Arguello A, Yang XY, Vogt D, Stanco A, Rubenstein JLR, Cheyette BNR. 2013. Dapper antagonist of catenin-1 cooperates with dishevelled-1 during postsynaptic development in mouse forebrain GABAergic interneurons. PLoS One. 8: e67679.

Arking DE, Cutler DJ, Brune CW, Teslovich TM, West K, Ikeda M, Rea A, Guy M, Lin S, Cook EH, et al. 2008. A common genetic variant in the neurexin superfamily member CNTNAP2 increases familial risk of autism. Am J Hum Genet. 82: 160–164.

Bakkaloglu B, O'Roak BJ, Louvi A, Gupta AR, Abelson JF, Morgan TM, Chawarska K, Klin A, Ercan-Sencicek AG, Stillman AA, et al. 2008. Molecular cytogenetic analysis and resequencing of contactin associated protein-like 2 in autism spectrum disorders. Am J Hum Genet. 82:165–173.

Chen J, Alberts I, Li X. 2014. Dysregulation of the IGF-I/PI3K/AKT/mTOR signaling pathway in autism spectrum disorders. Int J Dev Neurosci. 35:35–41.

Elia J, Gai X, Xie HM, Perin JC, Geiger E, Glessner JT, D'arcy M, deBerardinis R, Frackelton E, Kim C, et al. 2010. Rare structural variants found in attention-deficit hyperactivity disorder are preferentially associated with neurodevelopmental genes. Mol Psychiatry. 15:637–646.

Friedman JI, Vrijenhoek T, Markx S, Janssen IM, van der Vliet WA, Faas BH, Knoers NV, Cahn W, Kahn RS, Edelmann L, et al. 2008. CNTNAP2 gene dosage variation is associated with schizophrenia and epilepsy. Mol Psychiatry. 13:261–266.

Gogolla N, Leblanc JJ, Quast KB, Südhof TC, Fagiolini M, Hensch TK. 2009. Common circuit defect of excitatory-inhibitory balance in mouse models of autism. J Neurodev Disord. 1: 172–181.

Gordon A, Salomon D, Barak N, Pen Y, Tsoory M, Kimchi T, Peles E. 2016. Expression of Cntnap2 (Caspr2) in multiple levels of sensory systems. Mol Cell Neurosci. 70:42–53.

Han S, Tai C, Westenbroek RE, Yu FH, Cheah CS, Potter GB, Rubenstein JL, Scheuer T, de la Iglesia HO, Catterall WA. 2012. Autistic-like behaviour in Scn1a$^{+/-}$ mice and rescue by enhanced GABA-mediated neurotransmission. Nature. 489: 385–390.

Hashemi E, Ariza J, Rogers H, Noctor SC, Martínez-Cerdeño V. 2017. The number of Parvalbumin-expressing interneurons is decreased in the medial prefrontal cortex in Autism. Cereb Cortex. 13. doi:10.1093/cercor/bhx063.

Hashimshony T, Wagner F, Sher N, Yanai I. 2012. CEL-Seq: single-cell RNA-Seq by multiplexed linear amplification. Cell Rep. 27:666–673.

He M, Tucciarone J, Lee S, Nigro MJ, Kim Y, Levine JM, Kelly SM, Krugikov I, Wu P, Chen Y, et al. 2016. Strategies and tools for combinatorial targeting of GABAergic neurons in mouse cerebral cortex. Neuron. 91:1228–1243.

Hippenmeyer S, Vrieseling E, Sigrist M, Portmann T, Laengle C, Ladle DR, Silvia A. 2005. A developmental switch in the response of DRG neurons to ETS transcription factor signaling. PLoS Biol. 3:e159.

Hoffman EJ, Turner KJ, Fernandez JM, Cifuentes D, Ghosh M, Ijaz S, Jain RA, Kubo F, Bill BR, Baier H, et al. 2016. Estrogens suppress a behavioral phenotype in Zebrafish mutants of the Autism Risk Gene, CNTNAP2. Neuron. 89:725–733.

Horresh I, Poliak S, Grant S, Bredt D, Rasband MN, Peles E. 2008. Multiple molecular interactions determine the clustering of Caspr2 and Kv1 channels in myelinated axons. J Neurosci. 28:14213–14222.

Huang ZJ, Di Cristo G, Ango F. 2007. Development of GABA innervation in the cerebral and cerebellar cortices. Nat Rev Neurosci. 8:673–686.

Ji W, Li T, Pan Y, Tao H, Ju K, Wen Z, Fu Y, An Z, Zhao Q, Wang T, et al. 2013. CNTNAP2 is significantly associated with schizophrenia and major depression in the Han Chinese population. Psychiatry Res. 207:225–228.

Karayannis T, Au E, Patel JC, Kruglikov I, Markx S, Delorme R, Héron D, Salomon D, Glessner J, Restituito S, et al. 2014. Cntnap4 differentially contributes to GABAergic and dopaminergic synaptic transmission. Nature. 511:236–240.

Kawaguchi Y. 1993. Physiological, morphological, and histochemical characterization of three classes of interneurons in rat neostriatum. J Neurosci. 13:4908–4923.

Kawaguchi Y, Kubota Y. 1996. Physiological and morphological identification of somatostatin- or vasoactive intestinal polypeptide-containing cells among GABAergic cell subtypes in rat frontal cortex. J Neurosci. 16:2701–2715.

Kepecs A, Fishell G. 2014. Interneuron cell types are fit to function. Nature. 505:318–326.

Kessaris N, Magno L, Rubin AN, Oliveira MG. 2014. Genetic programs controlling cortical interneuron fate. Curr Opin Neurobiol. 26:79–87.

Madisen L, Garner AR, Shimaoka D, Chuong AS, Klapoetke NC, Li L, van der Bourg A, Niino Y, Egolf L, Monetti C, et al. 2015. Transgenic mice for intersectional targeting of neural sensors and effectors with high specificity and performance. Neuron. 85:942–958.

Madisen L, Zwingman TA, Sunkin SM, Oh SW, Zariwala HA, Gu H, Ng LL, Palmiter RD, Hawrylycz MJ, Jones AR, et al. 2010. A robust and high-throughput Cre reporting and characterization system for the whole mouse brain. Nat Neurosci. 13: 133–140.

Martins GJ, Shahrokh M, Powell EM. 2011. Genetic disruption of Met signaling impairs GABAergic striatal development and cognition. Neuroscience. 176:199–209.

Miyoshi G, Hjerling-Leffler J, Karayannis T, Sousa VH, Butt SJ, Battiste J, Johnson JE, Machold RP, Fishell G. 2010. Genetic fate mapping reveals that the caudal ganglionic eminence produces a large and diverse population of superficial cortical interneurons. J Neurosci. 30:1582–1594.

Patz S, Grabert J, Gorba T, Wirth MJ, Wahle P. 2004. Parvalbumin expression in visual cortical interneurons depends on neuronal activity and TrkB ligands during an Early period of postnatal development. Cereb Cortex. 14:342–351.

Paul A, Cai Y, Atwal GS, Huang ZJ. 2012. Developmental coordination of gene expression between synaptic partners during GABAergic circuit assembly in cerebral cortex. Front Neural Circuits. 26:37.

Paul A, Crow M, Raudales R, He M, Gillis J, Huang ZJ. In press. Transcriptional architecture of synaptic communication delineates cortical GABAergic neuron identity. Cell. bioRxiv: https://doi.org/10.1101/180034.

Peñagarikano O, Abrahams BS, Herman EI, Winden KD, Gdalyahu A, Dong H, Sonnenblick LI, Gruver R, Almajano J, Bragin A, et al. 2011. Absence of CNTNAP2 leads to epilepsy, neuronal migration abnormalities, and core autism-related deficits. Cell. 147:235–246.

Petrin AL, Giacheti CM, Maximino LP, Abramides DV, Zanchetta S, Rossi NF, Richieri-Costa A, Murray JC. 2010. Identification of a microdeletion at the 7q33-q35 disrupting the CNTNAP2 gene in a Brazilian stuttering case. Am J Med Genet A. 152A:3164–3172.

Poliak S, Gollan L, Martinez R, Custer A, Einheber S, Salzer JL, Trimmer JS, Shrager P, Peles E. 1999. Caspr2, a new member of the neurexin superfamily, is localized at the juxtaparanodes of myelinated axons and associates with K+ channels. Neuron. 24:1037–1047.

Poliak S, Salomon D, Elhanany H, Sabanay H, Kiernan B, Pevny L, Stewart CL, Xu X, Chiu SY, Shrager P, et al. 2003. Juxtaparanodal clustering of Shaker-like K+ channels in myelinated axons depends on Caspr2 and TAG-1. J Cell Biol. 162:1149–1160.

Poot M. 2015. Connecting the CNTNAP2 networks with neurodevelopmental disorders. Mol Syndromol. 6:7–22.

Poot M. 2017. Intragenic CNTNAP2 deletions: a bridge too far? Mol Syndromol. 8:118–130.

Poot M, Beyer V, Schwaab I, Damatova N, Van't Slot R, Prothero J, Holder SE, Haaf T. 2010. Disruption of CNTNAP2 and additional structural genome changes in a boy with speech delay and autism spectrum disorder. Neurogenetics. 11:81–89.

Potter GB, Petryniak MA, Shevchenko E, McKinsey GL, Ekker M, Rubenstein JLR. 2009. Generation of Cre-transgenic mice using Dlx1/Dlx2 enhancers and their characterization in GABAergic interneurons. Mol Cell Neurosci. 40:167–186.

Rodenas-Cuadrado P, Ho J, Vernes SC. 2014. Shining a light on CNTNAP2: complex functions to complex disorders. Eur J Hum Genet. 22:171–178.

Rodenas-Cuadrado P, Pietrafusa N, Francavilla T, La Neve A, Striano P, Vernes SC. 2016. Characterisation of CASPR2 deficiency disorder–a syndrome involving autism, epilepsy and language impairment. BMC Med Genet. 17:8.

Rubenstein JL, Merzenich MM. 2003. Model of autism: increased ratio of excitation/inhibition in key neural systems. Genes Brain Behav. 2:255–267.

Schrader LA, Birnbaum SG, Nadin BM, Ren Y, Bui D, Anderson AE, Sweatt JD. 2006. ERK/MAPK regulates the Kv4.2 potassium channel by direct phosphorylation of the pore-forming subunit. Am J Physiol Cell Physiol. 290:C852–C861.

Schrader LA, Ren Y, Cheng F, Bui D, Sweatt JD, Anderson AE. 2009. Kv4.2 is a locus for PKC and ERK/MAPK cross-talk. Biochem J. 417:705–715.

Selby L, Zhang C, Sun QQ. 2007. Major defects in neocortical GABAergic inhibitory circuits in mice lacking the fragile X mental retardation protein. Neurosci Lett. 412:227–232.

Sohal VS, Huguenard JR. 2005. Inhibitory coupling specifically generates emergent gamma oscillations in diverse cell types. Proc Natl Acad Sci USA. 102:18638–18643.

Stein MB, Yang BZ, Chavira DA, Hitchcock CA, Sung SC, Shipon-Blum E, Gelernter J. 2011. A common genetic variant in the neurexin superfamily member CNTNAP2 is associated with increased risk for selective mutism and social anxiety-related traits. Biol Psychiatry. 69:825–831.

Strauss KA, Puffenberger EG, Huentelman MJ, Gottlieb S, Dobrin SE, Parod JM, Stephan DA, Morton DH. 2006. Recessive symptomatic focal epilepsy and mutant contactin-associated protein-like 2. N Engl J Med. 354:1370–1377.

Südhof TC, Fagiolini M, Hensch TK. 2009. Common circuit defect of excitatory-inhibitory balance in mouse models of autism. J Neurodev Disord. 1:172–181.

Takano T. 2015. Interneuron dysfunction in syndromic autism: recent advances. Dev Neurosci. 37:467–475.

Taniguchi H, He M, Wu P, Kim S, Paik R, Sugino K, Kvitsani D, Fu Y, Lu J, Lin Y, et al. 2013. A resource of cre driver lines for genetic targeting of GABAergic Neurons in Cerebral Cortex. Neuron. 71:995–1013.

Varea O, Martin-de-Saavedra MD, Kopeikina KJ, Schürmann B, Fleming HJ, Fawcett-Patel JM, Bach A, Jang S, Peles E, Kim E, et al. 2015. Synaptic abnormalities and cytoplasmic glutamate receptor aggregates in contactin associated protein-like 2/Caspr2 knockout neurons. Proc Natl Acad Sci USA. 112:6176–6181.

Verkerk AJ, Mathews CA, Joosse M, Eussen BH, Heutink P, Oostra BA, Tourette Syndrome Association International Consortium for Genetics. 2003. CNTNAP2 is disrupted in a family with Gilles de la Tourette syndrome and obsessive compulsive disorder. Genomics. 82:1–9.

Vogt D, Cho KKA, Lee AT, Sohal VS, Rubenstein JLR. 2015. The parvalbumin/somatostatin ratio is increased in pten mutant mice and by human PTEN ASD Alleles. Cell Rep. 11:944–956.

Vogt D, Wu P-R, Sorrells SF, Arnold C, Alvarez-Buylla A, Rubenstein JLR. 2015. Viral-mediated Labeling and Transplantation of Medial Ganglionic Eminence (MGE) Cells for In Vivo Studies. J Vis Exp. 23:e52740. doi:10.3791/52740.

Vogt Weisenhorn DM, Celio MR, Rickmann M. 1998. The onset of parvalbumin-expression in interneurons of the rat parietal cortex depends upon extrinsic factor(s). Eur J Neurosci. 10:1027–1036.

Watson CM, Crinnion LA, Tzika A, Mills A, Coates A, Pendlebury M, Hewitt S, Harrison SM, Daly C, Roberts P, et al. 2014. Diagnostic whole genome sequencing and split-read mapping for nucleotide resolution breakpoint identification in CNTNAP2 deficiency syndrome. Am J Med Genet A. 164A:2649–2655.

Wen Y, Alshikho MJ, Herbert MR. 2016. Pathway network analyses for autism reveal multisystem involvement, major overlaps with other diseases and convergence upon MAPK and calcium signaling. PLoS One. 11:e0153329. Doi:10.1371/journal.pone.0153329.

Wonders CP, Anderson SA. 2006. The origin and specification of cortical interneurons. Nat Rev Neurosci. 7:687–696.

Xu Q, Tam M, Anderson SA. 2008. Fate mapping Nkx2.1-lineage cells in the mouse telencephalon. J Comp Neurol. 506:16–29.

Zhao YJ, Wang YP, Yang WZ, Sun HW, Ma HW, Zhao YR. 2015. CNTNAP2 is significantly associated with speech sound disorder in the Chinese Han population. J Child Neurol. 30:1806–1811.

Zweier C. 2012. Severe intellectual disability associated with recessive defects in CNTNAP2 and NRXN1. Mol Syndromol. 2:181–185.

Zweier C, de Jong EK, Zweier M, Orrico A, Ousager LB, Collins AL, Bijlsma EK, Oortveld MA, Ekici AB, Reis A, et al. 2009. CNTNAP2 and NRXN1 are mutated in autosomal-recessive Pitt-Hopkins-like mental retardation and determine the level of a common synaptic protein in Drosophila. Am J Hum Genet. 85:655–666.